Bi^{3+} acting both as an electron and as a hole trap in La-, Y-, and $LuPO_4$

Lyu, Tianshuai; Dorenbos, Pieter

DOI
10.1039/c8tc01020j

Publication date
2018

Document Version
Accepted author manuscript

Published in
Journal of Materials Chemistry C

Bi^{3+} acting both as electron and as hole trap in La-, Y-, and $LuPO_4$

Tianshuai Lyu* and Pieter Dorenbos

Delft University of Technology, Faculty of Applied Sciences, Department of Radiation Science and Technology, section Luminescence Materials, Mekelweg 15, 2629JB Delft, The Netherlands

E-mail: T.lyu-1@tudelft.nl

Abstract

Vacuum referred binding energy (VRBE)-guided design of Bi^{3+}-based storage and afterglow materials together with charge carrier trapping processes are explored with a study on bismuth and lanthanide doped rare earth ortho-phosphates. By combining Bi^{3+} with the shallow hole trap of Tb^{3+} or Pr^{3+}, Bi^{3+} appears to act as deep electron trap and as hole recombination center in YPO_4. By combining Bi^{3+} with the deep electron trap of Tm^{3+}, Sm^{3+}, Yb^{3+}, or Eu^{3+}, Bi^{3+} appears to act as shallow hole trap in YPO_4. Here recombination is also realized by means of hole release instead of more commonly reported electron release. Holes are released from Bi^{4+} and then recombine through the valence band with the electrons trapped at Ln^{2+} to produce Ln^{3+} 4f-4f emission. Lu^{3+} was introduced in YPO_4 to engineer the valence band (VB) energy and to tailor the hole trap depth of Bi^{3+} in $Y_{1-x}Lu_xPO_4$ solid solutions. The results show that with increasing x the VRBE at the valence band top moves downward and the hole trap depth of Bi^{3+} increases. With a deep understanding of Bi^{2+} and Bi^{3+} trap level locations and on the charge carrier trapping process, this work broadens the avenue to explore new persistent luminescence and storage materials by using Bi^{3+} both as electron and as hole trap.

1. Introduction

The research on trapping and transport of holes and electrons is of interest from a theoretical point of view[1-4] and because of potential applications in a variety of fields such as in night vision[5, 6], in-vivo bioimaging[7-9], information storage[10, 11], and alternating current light emitting diodes (AC-LEDs)[12]. To date few good persistent luminescence and storage phosphors were discovered, such as $SrAl_2O_4:Eu^{2+},Dy^{3+}$[5], $Zn_3Ga_2Ge_2O_{10}:Cr^{3+}$[8], and BaFBr: Eu^{2+}[13]. A trial and error method is often used to explore new materials, and there is a strong wish to have a tool that can guide us to deliberate design of storage and afterglow materials based on model prediction[2, 14].

The trapping and release process of holes is scarcely reported so far. Few of the examples are $MgS:Ce^{3+},Sm^{3+}$ by Chakrabarti et al. [15] in the 1980s and on YPO_4 by Lyu et al. [2] recently. The rare reporting on hole trapping and release processes is due to a lack of knowledge on how to identify a hole release process as compared to an electron release process. To address this issue we need the information on where the holes and electrons are located within the band gap. A model was published in 2012 to construct a vacuum referred binding energy (VRBE) diagram that shows the electron binding energies in the lanthanide levels when doped in inorganic compounds with respect to the vacuum level. It enables one to compare the VRBE at a defect level or a host band in different hosts with respect to the same reference energy[16-18]. Such model can be used to better identify the nature of trapping centers.

Like the Tl^+ and Pb^{2+} ions, the Bi^{3+} ion has a $6s^2$ electron configuration with $^1S_0$ ground state, while its excited states are singlet state $^1P_1$ and triplet states of $^3P_0$, $^3P_1$ and $^3P_2$ originating from the $6s^16p^1$ configuration. The excitation bands from the $^1S_0$ ground state to the $^3P_1$, $^3P_2$ and $^1P_1$ excited states are commonly referred to as A-, B-, and C-band[19]. Moreover, usually a broad excitation band appears, known as the D-band, which is due to the charge transfer from Bi^{3+} to the conduction band[20, 21].

Bi^{2+} as an activator has been reported in a few compounds. In 1994, Blasse et al. observed unusual orange luminescence in $SrB_4O_7:Bi^{2+}$[22]. Later, Bi^{2+} emission was observed in phosphates, sulphates, borates, and alkaline-earth fluorides for white light emitting diodes[23-26]. Recently Awater et al. reported the X-ray excited emission of Bi^{2+} in $Li_2BaP_2O_7$[27] and YPO_4[28]. Bi^{2+} has (Xe) $4f^{14}5d^{10}6s^26p^1$ configuration with ^2P ground state that can split into $^2P_{1/2}$ ground state and excited states of $^2S_{1/2}$, $^2P_{3/2}$ (1) and $^2P_{3/2}$ (2) through spin orbit and crystal field splitting[27]. Characteristic red emission of Bi^{2+} is attributed to the $^2P_{3/2}(1)\rightarrow{}^2P_{1/2}$ transition[26, 29].

Bismuth-based materials have attracted research interest for their various applications such as in electrocatalyst[30] and as high temperature superconductor[31]. Particularly, Bi^{3+} is an excellent activator and sensitizer for luminescent materials that has been studied during the past decades[27, 32-35]. There are rare reports regarding the persistent luminescence from bismuth, and only a few Bi^{3+}-doped afterglow phosphors have been discovered to date[36]. The literatures on Bi^{3+} acting as hole or as electron trap in afterglow and storage phosphors are summarized in Table 1. Rare reports are published to discuss the charge carrier trapping and

release processes in Bi^{3+}-doped phosphors and the mechanism always remains unidentified. The electron or hole release processes listed in Table 1 should be treated as indicative.

Katayama et al.[37] reported that Bi^{3+} related defects may act as electron trapping centers in the green persistent $Y_3Al_{5-x}Ga_xO_{12}$:0.005Ce^{3+},0.005Bi^{3+} phosphors. Here Ce^{3+} is the deep hole trapping center and electron donor. After exposure to 460 nm blue light, conduction band (CB) electrons generated through the photoionization process can be captured by Bi^{3+} to form Bi^{2+}. Under thermal excitation at RT, the electrons release gradually from Bi^{2+} to the conduction band and then recombine with Ce^{4+} to ultimately yield Ce^{3+} 5d-4f emission peaked at 505 nm. The electron trap depth produced by Bi^{3+} can be tuned by adjusting x from 0 to 4. The CB-bottom decreases and this demonstrates conduction band engineering.

Recently Zou et al.[38] suggest that Bi^{3+} may act as hole trapping and recombination center in the persistent phosphor of $NaLuGeO_4$:0.05Bi^{3+},0.005Cr^{3+}. Bi^{3+} is electron donor, and electrons generated through the photoionization process migrate through the conduction band to be trapped by 1.3 eV deep Cr^{3+} electron trap(s) to form Cr^{2+}. Under 980 nm laser excitation, the electrons release from Cr^{2+} to the conduction band and then recombine with Bi^{4+} to generate Bi^{3+} $^3P_1$-$^1S_0$ emission at 400 nm. Convincing evidence was not provided and not everything is fully clear in the charge carrier trapping and release process in Bi^{3+}-doped afterglow phosphors.

Table 1. Bi^{3+} acting as electron (e^-) or as hole (h^+) trap in afterglow and storage phosphors. The symbol $\leftarrow e^-$ means that electrons release at lower temperature than holes, while the symbol $h^+\rightarrow$ means holes release earlier than electrons.

Compound	h^+	transport	e^-	reference
Y_3Al_{5-}	Ce^{3+}	$\leftarrow e^-$	Bi^{3+}	[37]
$MgGeO_3$	Mn^{2+}	$\leftarrow e^-$	Bi^{3+}	[39]
$KGaGeO_4$	host defects	$h^+\rightarrow$	Bi^{3+}	[36]
CaS	host defects	$h^+\rightarrow$	Bi^{3+}	[40]
$CaWO_4$	Bi^{3+}	$\leftarrow e^-$	$Bi_{Ca}^{\bullet}$	[41]
$NaLuGeO_4$	Bi^{3+}	$\leftarrow e^-$	Cr^{3+}	[38]
$NaLuGeO_4$	Bi^{3+}	$\leftarrow e^-$	Eu^{3+}	[42]
$SrGa_2O_4$	Bi^{3+}	$\leftarrow e^-$	host defects	[43]
$CaGa_2O_4$	Bi^{3+}	$\leftarrow e^-$	host defects	[44]
$CdSiO_3$	Bi^{3+}	$\leftarrow e^-$	host defects	[45]

The objective of the study is to systematically reveal the charge carrier trapping process and to explore deliberate design of bismuth-doped storage and afterglow phosphors based on VRBE diagram predictions and band gap engineering. $REPO_4$ (RE=La, Y, and Lu) are used as model compounds because there is only one crystallographic RE^{3+} site that can be easily substituted by Bi^{3+} and trivalent lanthanides. Fig. 1 shows the ground state energies of both Bi^{2+} and Bi^{3+} in the vacuum referred binding energy diagram of YPO_4 as presented by Awater et al. in Ref [28]. Such a VRBE scheme provides a powerful predictive tool. For instance, it predicts that Bi^{3+} can act as a 1.80 eV deep hole trap to generate Bi^{4+} but also as a 2.70 eV deep electron trap to form Bi^{2+}. When combining Bi^{3+} with more than 1.80 eV deep electron

trapping centers like Eu^{3+}, Sm^{3+}, Yb^{3+}, or Tm^{3+}, the holes will release from Bi^{4+} earlier, i.e., at lower temperature, than the electrons from Eu^{2+}, Sm^{2+}, Yb^{2+}, or Tm^{2+} to generate Ln^{3+} 4f-4f emission. In this work we will test those type of predictions and provide therewith also an independent confirmation of the results in Awater et al. [28].

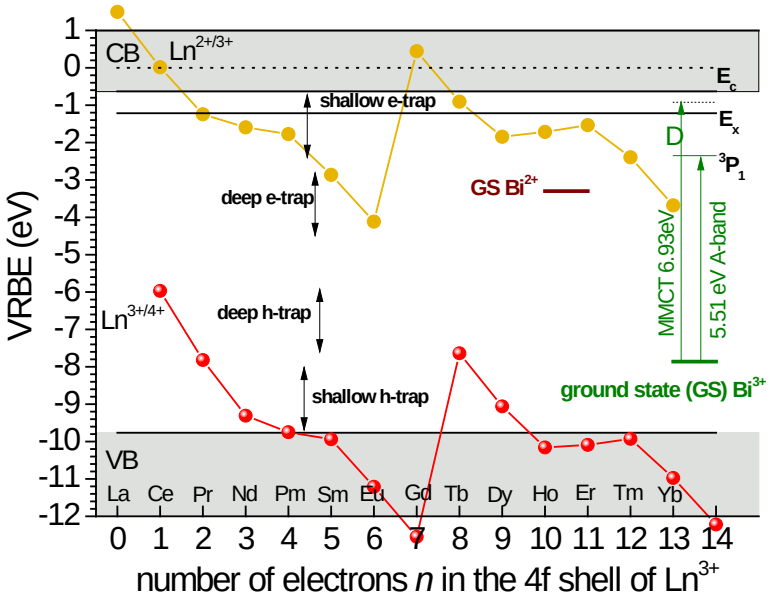

Fig. 1. VRBE scheme for YPO_4 including lanthanide, Bi^{3+}, and Bi^{2+} energy level locations. E_c is the binding energy at the conduction band bottom and E_x is the binding energy in the host exciton. The Bi^{3+}→CB metal-to-metal charge transfer (MMCT) band D and the $^3P_1$ excited state of Bi^{3+} are also shown.

2. Experimental

All starting chemicals were purchased from Sigma-Aldrich and utilized without further treatments. Samples were synthesized by a conventional high temperature solid state reaction. Appropriate stoichiometric mixtures of Bi_2O_3 (99.999%), $NH_4H_2PO_4$ (99.99%) and rare earth oxides (99.999%) were mixed well with the help of acetone. Subsequently, it was put into a corundum crucible and fired at 400 ^oC for 5 h and then at 1400 ^oC for 10 h under ambient atmosphere. After that, the obtained samples were cooled to room temperature (RT) and milled homogeneously before further measurements.

The crystal structure determination of all samples was performed on a PANalytical XPert PRO X-ray diffraction system with a cobalt (Co) Kα (λ=0.178901 nm) X-ray tube (45 KV, 30 mA). The photoluminescence emission (PL) and PL excitation (PLE) spectra were collected on equipment with a VUV/UV branch utilizing a deuterium lamp and an ARC VM502 vacuum monochromator. The emission was detected using a photomultiplier of PerkinElmer Photon Counting Module (MP-1913). The sample temperature was controlled utilizing a closed cycle helium cryostat (HC-4) and a Lake Shore 331 temperature controller. All PLE spectra were corrected for the incident photon flux intensity.

TL recordings above room temperature were recorded with a RISØ TL/OSL reader (Model DA-15) and a DA-20 controller. Samples were first heated to 900 K to empty all relevant traps, and then cooled to room temperature followed by β irradiation using a $^{90}Sr/^{90}Y$ source at a dose rate of ~0.7 mGy/s in complete darkness. All TL recordings were collected under a flow of nitrogen (N_2) gas and the heating rate is always 1 K/s. A 600 nm bandpass filter (600FS40-50) was placed between the PM tube and the sample to select red emission from Eu^{3+} or Sm^{3+}. In order to select the ultraviolet emission from Bi^{3+} or blue emission from Tm^{3+}, 239 nm bandpass (239FS10-50) and 450 nm bandpass (450FS20-50) filters were used, respectively.

Prior to the recording of the low-temperature TL (LTTL) glow curves (90-450 K), the samples were first heated to 450 K for 3 min to empty all relevant traps and then cooled to 90 K followed by 600 s β irradiation using a $^{90}Sr/^{90}Y$ beta source at a dose rate of ~0.4 mGy s^{-1}. Liquid nitrogen was utilized as the cooling medium. Each powder sample was pressed into a pill with 0.4 cm diameter, mass <10 mg, and area ~0.2 cm^2. The pill was attached to the cold finger with heating element using silver paint. LTTL measurements were carried out at a heating rate of 1 K/s under vacuum (10^{-7} mbar). The Eu^{3+} emission was monitored by using a 600 nm bandpass filter (600FS40-50) and a PerkinElmer channel PM tube (MP-1393).

For the TL emission (TLEM) spectra, the samples were first heated to 800 K 3 times to empty all relevant traps and then exposed to gamma ray irradiation from a ^{60}Co source to an absorbed dose of ~1 kGy. TL emission was recorded at a heating rate of 1 K/s utilizing a UV to VIS spectrometer (Ocean Optics, QE65000) and a NIR spectrometer (Ocean Optics, NIRQ512) with a HR composite grating (300 lines/mm) and an entrance aperture of 100 μm leading to a wavelength resolution of 3.3 nm (fwhm). The spectral range is 200-900 nm for QE65000 and for NIRQ512 it is 900-1700 nm.

TL excitation (TLE) spectra were recorded by first charging the samples during 600 s with a laser beam produced by a tuneable diode pumped laser system (NT230-100-SH/DUV-SCU). A fiber FBPI600660710/2M purchased from Polymicro Technologies was utilized to transport the laser beam to the RISØ TL/OSL reader. A program was used to record TL glow curves between 300-750 K at a heating rate of 5 K/s when the excitation wavelengths change between 210 and 260 nm. A plot of the integrated intensity of a TL glow peak against illumination wavelength is defined as the TL excitation spectrum of that glow peak[46, 47]. The TLE spectra were finally corrected for the intensity of the laser and the typical transmittance of the fiber and used polarizer. A 600 nm bandpass filter 600FS40-50 was used to select Eu^{3+} emission.

3. Results

3.1. X-ray diffraction and photoluminescence spectroscopy

The synthesized samples of $Y_{1-x}Lu_xPO_4$:0.005Eu^{3+},0.005Bi^{3+} form nice solid solutions without any indications for an impurity phase as is evidenced with the XRD patterns in Fig. S1.

Fig. 2 shows the PL and PLE spectra of La-, Y-, and $LuPO_4$ phosphates recorded at 10 K. Under 166 nm host exciton excitation $LuPO_4$:0.005Bi^{3+} shows a strong emission band at ~248 nm and weak emission at ~326 nm. A similar spectrum appears under Bi^{3+} A-band excitation at 225 nm, see Fig. S2d. Like YPO_4 in Ref [48], and considering that Y-, and $LuPO_4$ have the same crystal structure, we assign the 248 and 326 nm bands to Bi^{3+} $^3P_1 \rightarrow {}^1S_0$ A-band and Bi-pair emission, respectively. Monitoring 248 nm and 326 nm emission, an excitation band at 225 nm appears in Fig. 2b. Like in the study from Srivastava et al. [48], this band is assigned to the Bi^{3+} A-band. In addition to that work we also performed VUV measurements that reveal the $^1S_0 \rightarrow {}^1P_1$ C-band at 166 nm in Fig. 2b. The broad band around 179 nm is like for YPO_4 in Ref [28, 49] attributed to the $Bi^{3+} \rightarrow$CB charge transfer band or D-band.

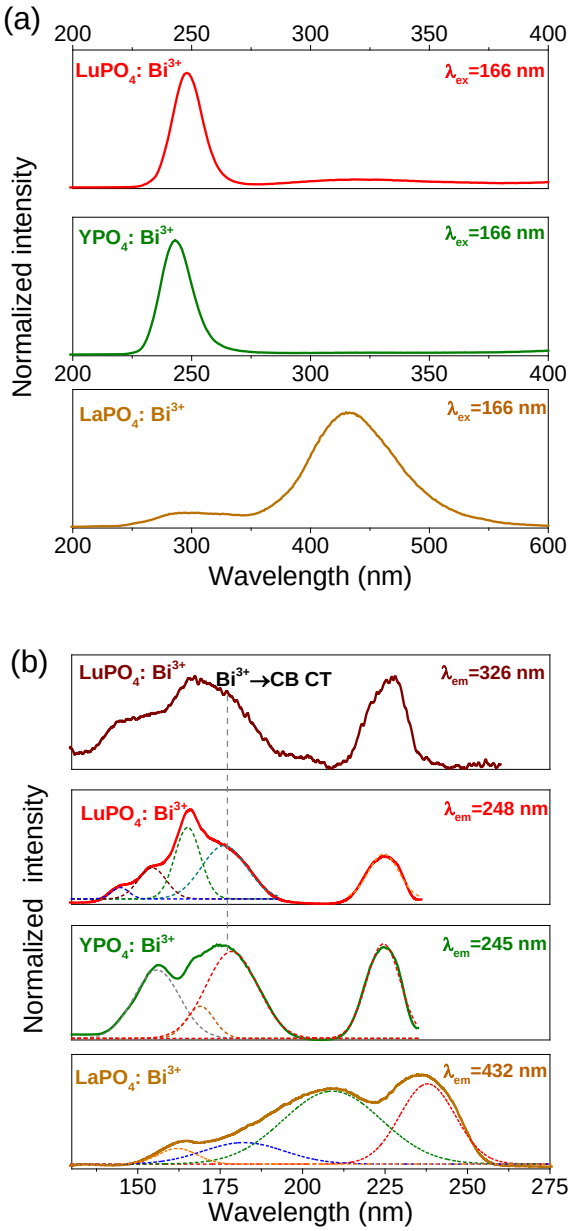

Fig. 2. (a) Photoluminescence (PL) and (b) PL excitation (PLE) spectra of $REPO_4$:0.005Bi^{3+} (RE=Lu and Y) and $LaPO_4$:0.002Bi^{3+} under 166 nm excitation at 10 K.

The PLE spectrum of $LaPO_4$:0.002Bi^{3+} monitoring at 432 nm in Fig. 2b is less well-structured than that of YPO_4 and $LuPO_4$. The band at 238 nm is tentatively attributed to the Bi^{3+} $^1S_0 \rightarrow {}^3P_1$ transition. Bands C and D cannot be distinguished and instead a broad unstructured band extends from below 175 nm to above 225 nm. $LaPO_4$:0.002Bi^{3+} shows a broad emission near 432 nm, which is attributed to CB→Bi^{3+} charge transfer emission. The host exciton creation band in $LaPO_4$ is known to be located near 155 nm[50-52]. It does, like in Moncorge et al. [53], not appear in the Bi^{3+} excitation spectrum indicating inefficient energy transfer.

3.2. Bi^{3+} as deep electron trap in Y-Lu phosphate solid solutions

It was shown in Ref. [2] that the trap depths of Tb^{3+} and Pr^{3+} hole trapping centers are shallower than those deep electron trapping centers of Ln^{3+} (Ln=Yb, Sm, and Eu) in YPO_4. When co-doping Ln^{3+} with Tb^{3+} or Pr^{3+}, the holes trapped by Tb^{4+} or Pr^{4+} will release at lower temperature to recombine with electrons trapped at Ln^{2+}, generating two characteristic TL glow peaks named IIIa (Tb) and IIIb (Pr) with emission from Ln^{3+}. These all were tested in Ref. [2]. For illustrating these hole release processes the results are reproduced for the Yb^{3+}, Pr^{3+} combination in Fig. 3b. The holes trapped by Pr^{4+} are released to recombine with electrons at Yb^{2+}, which yields a typical IIIb (Pr) glow peak with Yb^{3+} $^2F_{5/2} \rightarrow {}^2F_{7/2}$ emission. Let us now turn to the Bi^{3+}-doped YPO_4 compounds. Like Yb^{3+}, Bi^{3+} also can act as a deep electron trapping center in YPO_4, which will be discussed later. When combining Bi^{3+} with Pr^{3+}, then the holes trapped by Pr^{4+} will release earlier to recombine with electrons at Bi^{2+} producing Bi^{3+} A-band emission in YPO_4:0.005Bi^{3+},0.005Pr^{3+} as shown in Fig. 3a. The same now applies to solid solutions $Y_{1-x}Lu_xPO_4$:0.005Bi^{3+} codoped with 0.005Tb^{3+} or Pr^{3+} as in Fig. S3d) and e). Like for Yb^{3+}, Sm^{3+}, and Eu^{3+} ions, it appears that Bi^{3+} also acts as an electron trap in $Y_{1-x}Lu_xPO_4$ compounds with trap depth that is deeper than the hole trap of Pr^{3+} and Tb^{3+}.

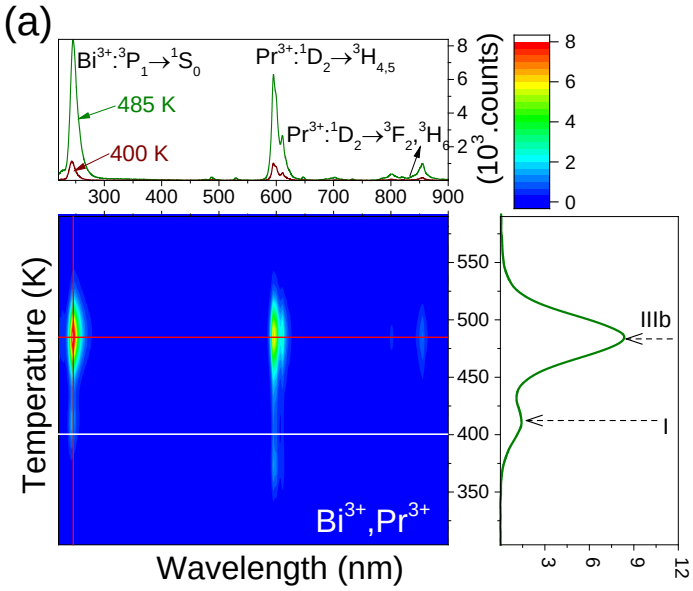

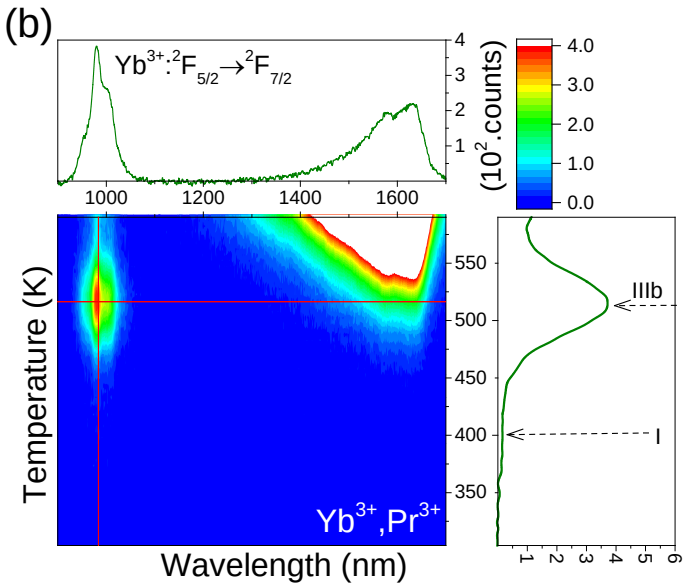

Fig. 3. Thermoluminescence emission (TLEM) plots of (a) YPO_4:0.005Bi^{3+},0.005Pr^{3+} and (b) YPO_4:0.005Yb^{3+},0.005Pr^{3+} recorded at a heating rate of 1 K/s. The data on Yb^{3+}-Pr^{3+}-codoped YPO_4 were obtained from Lyu et al. [2].

Fig. 4a) or b) shows the TL glow curves for solid solutions $Y_{1-x}Lu_xPO_4$:0.005Bi^{3+} codoped with 0.005Tb^{3+} or Pr^{3+}. When x increases, peaks IIIa and IIIb shift 40 K towards higher temperature. Similar peaks IIIa and IIIb shifting was reported by Lyu et al.[2] on $Y_{1-x}Lu_xPO_4$:0.005Ln^{3+},0.005Tb^{3+} or Pr^{3+} (Ln=Yb, Sm, and Eu), where the shifting of peaks IIIa and IIIb was attributed to increased activation energy for hole release from Tb^{4+} and Pr^{4+} due to valence band lowering with increasing x. Upon replacing Ln^{3+} (Ln=Yb, Sm, and Eu) for Bi^{3+} in $Y_{1-x}Lu_xPO_4$:0.005Bi^{3+}, a hole release process from Tb^{4+} or Pr^{4+} still occurs, and the only difference is that TL emission is now from Bi^{3+} instead of from Yb^{3+}, Sm^{3+}, or Eu^{3+}. Note that peak I at ~410 K, that was attributed to hole release from an intrinsic defect in [2], remains at constant temperature when x changes.

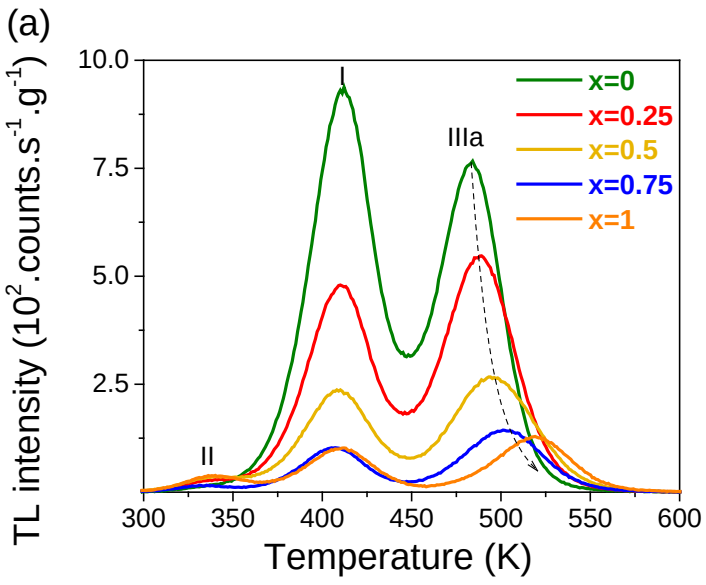

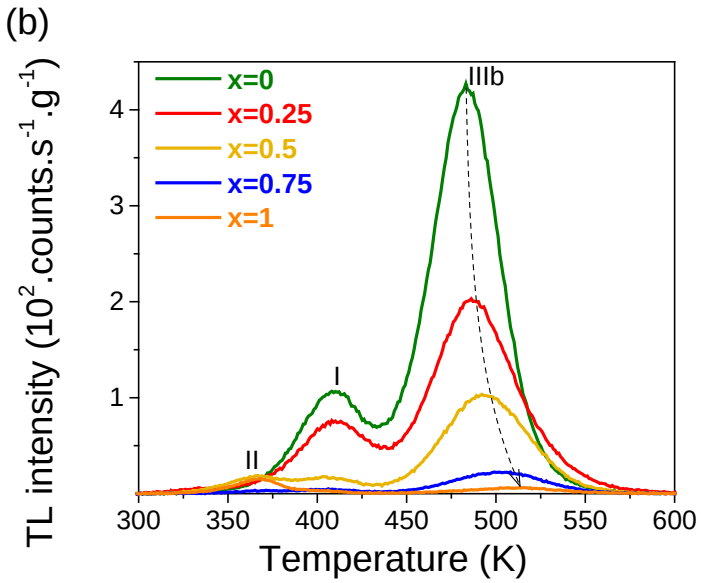

Fig. 4. TL glow curves of (a) $Y_{1-x}Lu_xPO_4$:0.005Bi^{3+},0.005Tb^{3+} and (b) $Y_{1-x}Lu_xPO_4$:0.005Bi^{3+}, 0.005Pr^{3+} (x=0-1) monitoring Bi^{3+} emission recorded at a heating rate of 1 K/s.

3.3. Engineering Bi^{4+} hole release in Y-Lu phosphate solid solutions

Based on the vacuum referred binding energy diagram of YPO_4 as shown in Fig. 1, we combined Bi^{3+} with the deep electron trap Eu^{3+} to verify the role of Bi^{3+} as hole trapping and hole release center. Fig. 5 shows a characteristic TL emission plot for YPO_4:0.005Eu^{3+}, 0.005Bi^{3+}. Weak Bi^{3+} emission is observed and 100 times stronger Eu^{3+} 4f-4f emission appears. This shows that Eu^{3+} is the dominant recombination and luminescence center and we deal with hole release during recombination. TL emission plots for three $LaPO_4$ samples with combinations of Bi^{3+} and Ln^{3+} can be found in Fig. S7.

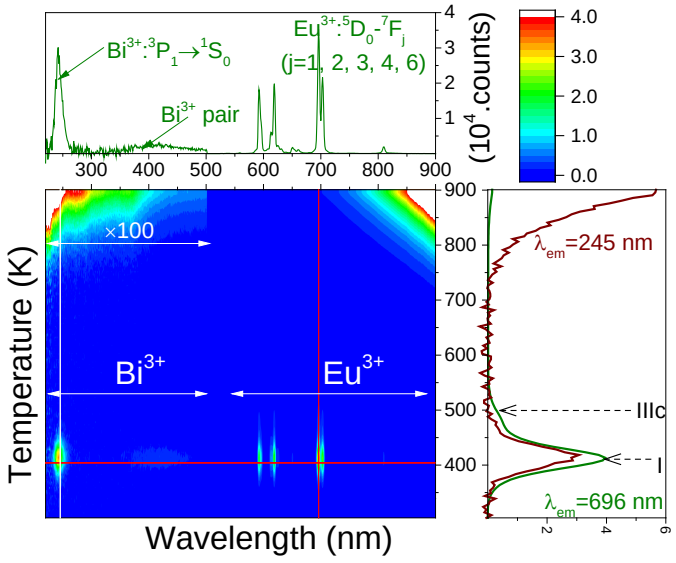

Fig. 5. Thermoluminescence emission (TLEM) plot of YPO_4:0.005Eu^{3+},0.005Bi^{3+} recorded at a heating rate of 1 K/s.

Like Eu^{3+}, the VRBE scheme of YPO_4 in Fig.1 also predicts that Sm^{3+}, Tm^{3+}, and Yb^{3+} act as deep electron traps. Samples of them combined with Bi^{3+} will help to study the hole release process from Bi^{4+}. Fig. 6 shows the TL glow curves of YPO_4:0.005Bi^{3+} and YPO_4: 0.005Ln^{3+},0.005Bi^{3+} (Ln=Sm, Eu, and Tm) samples. For YPO_4:0.005Yb^{3+},0.005Bi^{3+} a TL emission plot is shown in Fig. S3j. The glow peak at ~490 K for YPO_4:0.005Bi^{3+}, which will be referred to as peak IIIc, is also observed for YPO_4:0.005Sm^{3+},0.005Bi^{3+}, YPO_4:0.005Eu^{3+}, 0.005Bi^{3+}, YPO_4:0.005Tm^{3+},0.005Bi^{3+}, and YPO_4:0.005Yb^{3+},0.005Bi^{3+}. Peak IIIc is absent in the Sm^{3+} and Eu^{3+} single doped samples. Note that all Bi^{3+}-doped samples share peak I at ~417 K, which shifts ~5-15 K towards higher temperature as compared to Sm^{3+} or Eu^{3+} single doped samples. This may be attributed to unidentified modification of trap(s) for peak I with Bi^{3+} co-doping. Peak IV seems to be present only in Eu^{3+} doped samples. This all suggests that peaks IIIc is related to hole release and to the presence of Bi^{3+}.

Assuming first-order TL-recombination kinetics, the trap depths in the YPO_4:0.005Ln^{3+}, 0.005Bi^{3+} sample were estimated by employing the peak maximum (T_m) of the TL glow curve and solving[54-57]

$$\frac{\beta E}{kT_m^{\,2}} = s \times \exp\left(-\frac{E}{kT_m}\right) \qquad (1)$$

where β=1 K s^{-1} is the heating rate, E (eV) is the trap depth, k denotes the Boltzmann constant, and s (s^{-1}) is the frequency factor. Since the concentration of Bi^{3+} is low, we assume that the obtained frequency factors for $Y_{1-x}Lu_xPO_4$:0.005Eu^{3+},0.005Tb^{3+} found in Ref. [2] by variable heating rate plots also apply to $Y_{1-x}Lu_xPO_4$0.005Ln^{3+},0.005Bi^{3+}. The frequency factors s, and derived trap depths are listed in column 2, and 4 of Table 2.

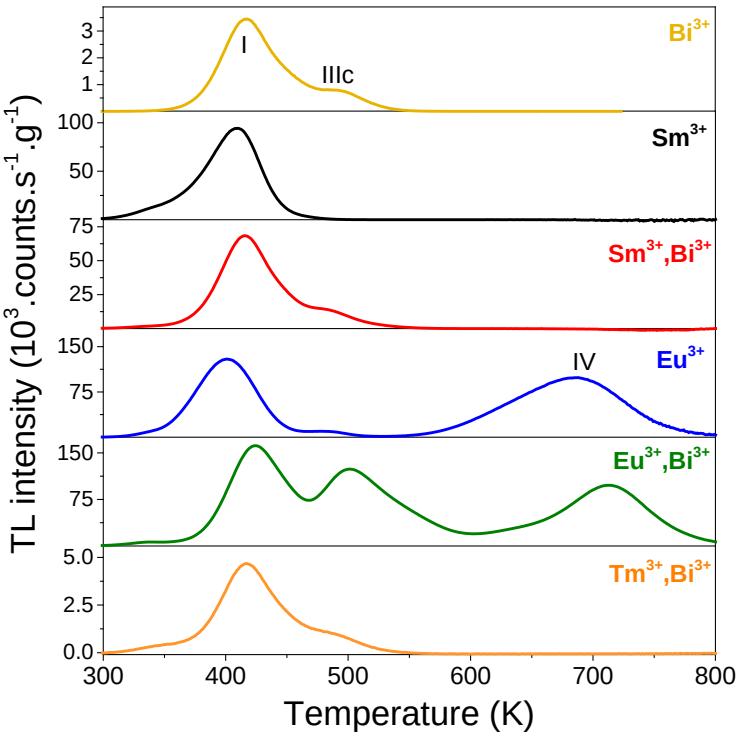

Fig. 6. TL glow curves of YPO_4:0.005Ln^{3+},0.005Bi^{3+} (Ln=Sm, Eu, and Tm) recorded after 2000 s β irradiation monitoring the emission from Sm^{3+}, or from Eu^{3+} and Tm^{3+} at a heating rate of 1 K/s. For YPO_4:0.005Bi^{3+} a 239 nm bandpass filter was used to select Bi^{3+} emission.

Table 2. TL results for $REPO_4$:0.005Ln^{3+},0.005Bi^{3+} (RE=Y, Lu, and La) samples providing the frequency factor s (s^{-1}), and the trap depths E (eV) for TL glow peak IIIc.

Compound	s	Ln^{3+}	Bi E(IIIc)
YPO_4	1.45×10^{13}	Sm^{3+}	1.39
YPO_4	1.45×10^{13}	Tm^{3+}	1.39
YPO_4	1.45×10^{13}	Eu^{3+}	1.42
YPO_4	1.45×10^{13}	Yb^{3+}	1.37
$Y_{0.75}Lu_{0.25}PO_4$	4.45×10^{13}	Eu^{3+}	1.53
$Y_{0.5}Lu_{0.5}PO_4$	2.53×10^{14}	Eu^{3+}	1.66
$Y_{0.25}Lu_{0.75}PO_4$	1.29×10^{15}	Eu^{3+}	1.78
$LuPO_4$	1.03×10^{15}	Eu^{3+}	1.79
$LaPO_4$	2.14×10^{12}	Eu^{3+}	0.54

Compared with YPO_4, the valence band bottom is at ~0.1 eV lower energy in $LuPO_4$. If the Bi^{3+} ground state remains stationary on the VRBE scale, the hole release from Bi^{4+} is predicted to occur at about 30-40 K higher temperature in $LuPO_4$. Fig. 7a shows the TL glow curves of $Y_{1-x}Lu_xPO_4$:0.005Bi^{3+},0.005Eu^{3+} solid solutions. With increasing x peak IIIc shifts 56 K towards higher temperature but peak I remains constant. A similar peak shifting of about 66 K was identified in $Y_{1-x}Lu_xPO_4$:0.005Eu^{3+},0.005Pr^{3+} in the study by Lyu et al. [2]. Peak IIIb in Fig. 7b was attributed to hole release from Pr^{4+}, and the hole trapping depth increases with x. The trapping parameters were derived using T_m as observed in Fig. 7a and solving Eq. (1) at β=1 K/s. The results are compiled in column 4 of Table 2.

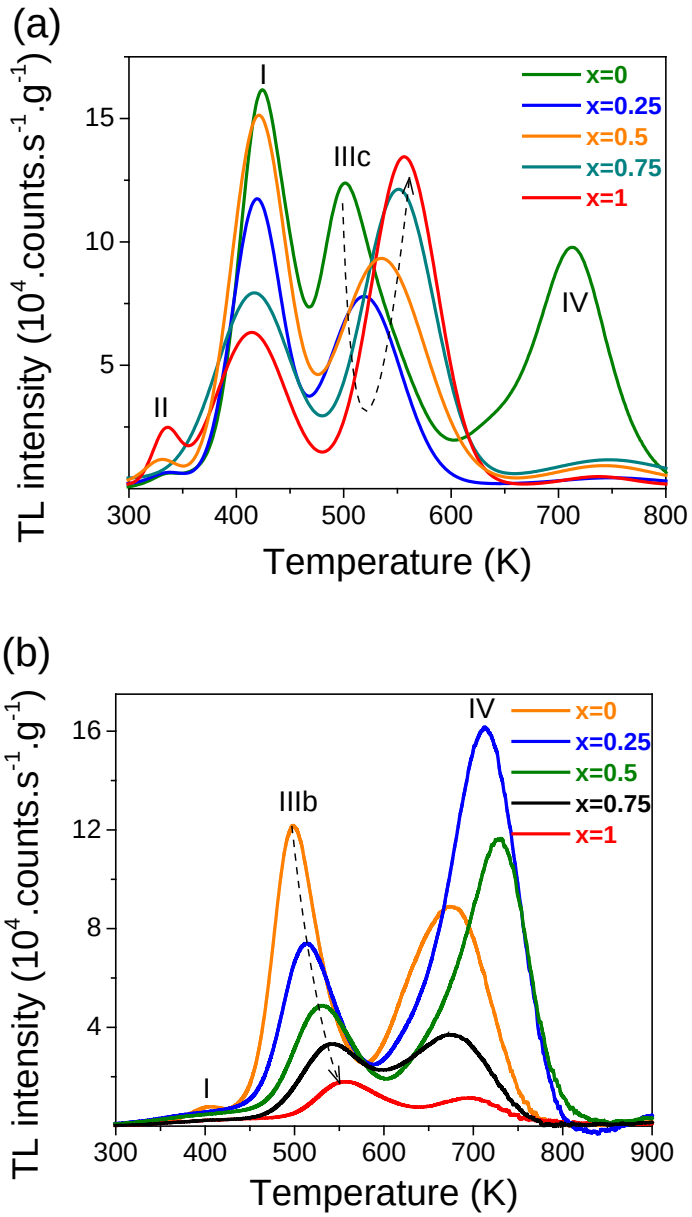

Fig. 7. TL glow curves for (a) $Y_{1-x}Lu_xPO_4$:0.005Eu^{3+},0.005Bi^{3+} and (b) $Y_{1-x}Lu_xPO_4$:0.005Eu^{3+}, 0.005Pr^{3+} solid solutions monitoring the emission from Eu^{3+} recorded at a heating rate of 1 K/s. The data on Eu^{3+}-Pr^{3+}-codoped samples were obtained from Lyu et al. [2].

For $LaPO_4$ it is known that the valence band top is at 0.77 eV higher energy than in YPO_4 [2]. Again assuming that the VRBE in the Bi^{3+} ground state is more or less invariant, hole release from Bi^{4+} is expected to occur at about 320 K lower temperature which would be near 200 K. Therefore a low temperature TL-study was performed. Fig. 8 shows the low temperature TL (LTTL) glow curves of $LaPO_4$:0.005Eu^{3+},0.005Bi^{3+} and $LaPO_4$:0.005Eu^{3+}, 0.005Ln^{3+} (Ln=Tb, and Ce). Similar as peak IIIa attributed to hole release from Tb^{4+} in $LaPO_4$ [2], Bi^{3+} gives rise to a glow peak at the predicted temperature near 206 K that is referred to as IIIc. The LTTL glow curve of $LaPO_4$:0.005Eu^{3+},0.005Ce^{3+} is shown to demonstrate the absence of peaks IIIa and IIIc. Considering that the content of Bi^{3+} is low, we

assume that the determined frequency factor for $LaPO_4$:0.005Eu^{3+},0.005Tb^{3+} found in Ref. [2] using variable heating rate plots also applies to $LaPO_4$:0.005Eu^{3+},0.005Bi^{3+}. The activation energy compiled in column 4 of Table 2 for glow peak IIIc was determined utilizing Eq. (1) and T_m as observed in Fig. 8 at β=1 K/s.

The glow peaks appearing above room temperature were also further investigated and are shown in Fig. S8, and S9. $LaPO_4$:0.005Eu^{3+},0.005Bi^{3+} with the most intense glow peak IIc close to RT also shows the most intense Eu^{3+} afterglow luminescence in Fig. S10a, which can still be detected after 12 h. In addition Fig. S11 shows a TL excitation (TLE) spectrum of the TL glow peak between 300-500 K of $LaPO_4$:0.005Eu^{3+},0.005Bi^{3+} in order to reveal the origin of glow peaks I and IIc.

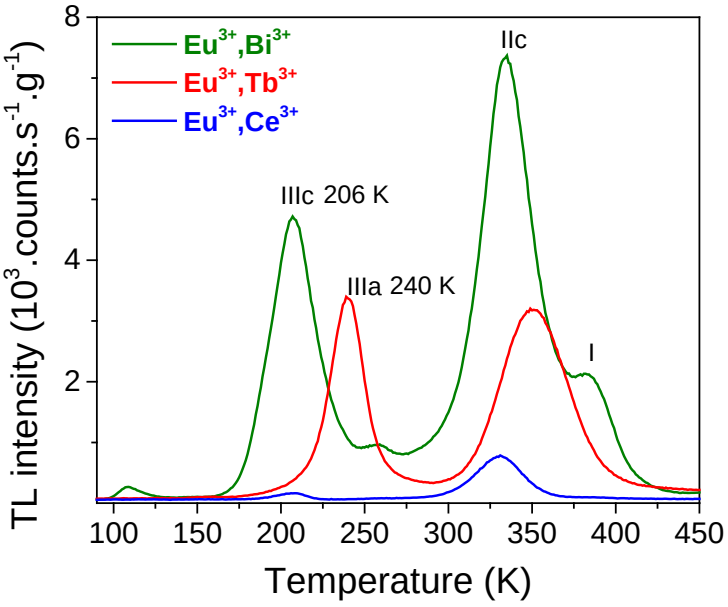

Fig. 8. Low-temperature TL (LTTL) glow curves of $LaPO_4$:0.005Eu^{3+},0.005Bi^{3+} and $LaPO_4$:0.005Eu^{3+},0.005Ln^{3+} (Ln=Tb, and Ce) monitoring the Eu^{3+} emission at a heating rate of 1 K/s. The data on $LaPO_4$:0.005Eu^{3+},0.005Ln^{3+} were obtained from Lyu et al. [2].

To study the origin of glow peak IIIc for the Bi^{3+}, Eu^{3+} combination in Fig. 5 and 6, the thermoluminescence excitation (TLE) spectrum of the TL glow peak between 470-600 K of YPO_4:0.005Eu^{3+},0.005Bi^{3+} was recorded and shown in Fig. 9. A broad TL excitation band extending from 210 to 260 nm is observed. The position resembles the onset of Eu^{3+} CT-band of Eu^{3+} single doped YPO_4 at 210-260 nm also shown in Fig. 9. This shows that after Eu^{3+} CT-band excitation, the holes created in the valence band are captured by Bi^{3+} that is responsible for the TL glow peak IIIc.

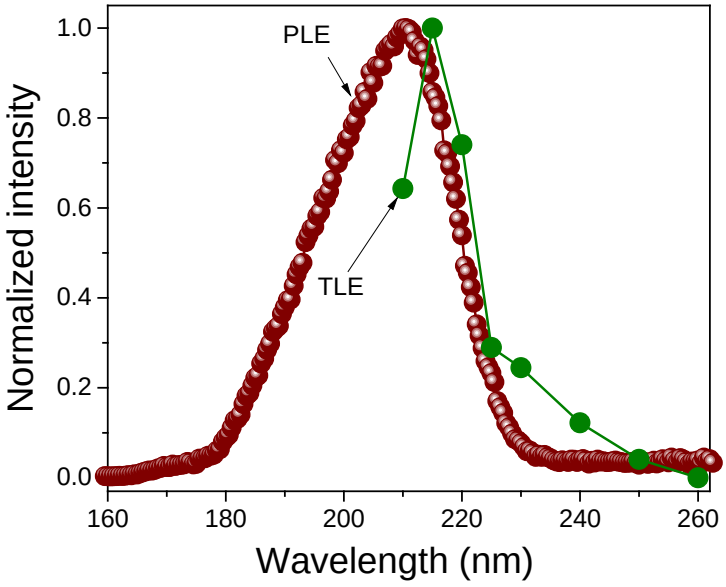

Fig. 9. Thermoluminescence excitation (TLE) spectrum of YPO_4:0.005Eu^{3+},0.005Bi^{3+} and photoluminescence excitation (PLE) spectrum of YPO_4:0.005Eu^{3+} monitoring the Eu^{3+} 592 nm emission recorded at room temperature.

4. Discussion

The vacuum referred binding energy (VRBE) diagram containing lanthanide, Bi^{3+} and Bi^{2+} energy levels will first be interpreted, and then we will show how it can be utilized to control the hole trapping and detrapping processes in bismuth and lanthanide co-doped rare earth ortho-phosphates.

Fig. 10 shows the stacked VRBE diagram of lanthanide doped La-, Y-, and $LuPO_4$ from our previous study [2], together with the Bi^{3+} and Bi^{2+} ground state locations based on this work. To determine the VRBE in the $6s^2$ ground state of Bi^{3+}, the metal-to-metal charge transfer (MMCT) energy of an electron from Bi^{3+} to the conduction band, as measured in Fig. 2b are used. The Bi^{3+}→CB CT-bands in $REPO_4$ (RE=Y, and Lu) are at 179 nm, and 176 nm, respectively. This energy, see arrow D in Fig. 1, is defined as the energy difference between the Bi^{3+} ground state and the energy in between the conduction band bottom and E_x. One then obtains -7.9, and -8 eV for the VRBE in the Bi^{3+} ground states of $REPO_4$:0.005Bi^{3+} (RE=Y, and Lu), respectively. The study from Awater et al. [19] showed that the VRBE in the Bi^{3+} $^1S_0$ ground state in oxide compounds is found between -5 and -10 eV and for phosphates it is always near -8 eV. Also considering that $REPO_4$ (RE=La, Y, and Lu) are quite similar, we expect that the VRBE in the Bi^{3+} $^1S_0$ ground state in $LaPO_4$ will be located between -7 and -9 eV and at the Bi^{3+}→CB CT-band between 150 and 200 nm. This is consistent with the fitted Gaussian band at around 180 nm in Fig. 2b that is then assumed to be the Bi^{3+}→CB CT-band. The Bi^{3+} ground state is then determined at -7.7±0.3 eV for $LaPO_4$. It should be noticed that the Bi^{3+} MMCT-band for $LaPO_4$ obtained in this work should be treated as indicative. From the Bi^{2+} radioluminescence in YPO_4 in Ref [28], the VRBE in the $^2P_{1/2}$ ground state of

Bi^{2+} in YPO_4 is estimated at -3.3 eV. Considering that La-, Y-, and $LuPO_4$ are quite similar and the VRBE in the Bi^{2+} ground states in oxide compounds are estimated near -3.5 eV in Ref [58], like Bi^{2+} in YPO_4, we then expect the Bi^{2+} ground states at -3.3±0.5 eV for other $REPO_4$ (RE=La, and Lu). Details about how to construct the VRBE diagram from spectroscopic data can be found in Refs [16, 18].

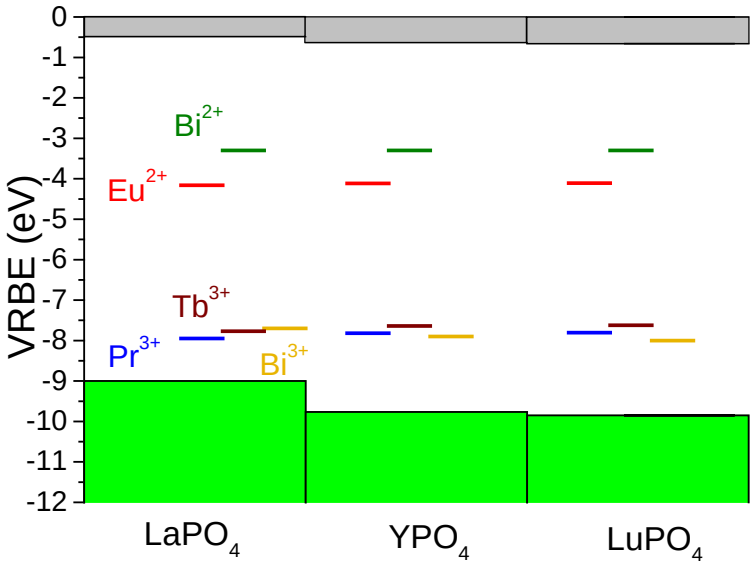

Fig. 10. Stacked VRBE diagram of $REPO_4$ (RE=La, Y, and Lu) with the vacuum referred binding energy in the ground states of Eu^{2+}, Pr^{3+}, Tb^{3+}, Bi^{2+}, and Bi^{3+}.

4.1. Bi^{3+} as deep electron trap combined with shallow hole trapping centers

The stacked vacuum referred binding energy (VRBE) scheme of YPO_4 in Fig. 10 predicts that the holes captured by Pr^{4+} and Tb^{4+} will be released earlier, i.e., at lower temperature than the electrons captured at Bi^{2+} to produce the characteristic emission of Bi^{3+}.

Fig. 3a and S3b-c shows the TL emission plots for YPO_4 each with the same Bi^{3+} electron trapping center but with different hole trapping centers Pr^{3+}, Ce^{3+}, and Tb^{3+}. Contrary to YPO_4: $0.005Bi^{3+}$,$0.005Ce^{3+}$ with the 3.80 eV deep hole trap on Ce^{3+}, YPO_4:$0.005Bi^{3+}$, $0.005Tb^{3+}$ or Pr^{3+} show glow peaks IIIa and IIIb due to hole release from Tb^{4+} and Pr^{4+} with trap depths of about 1.4 eV. Apparently the electron trap of Bi^{3+} is much deeper which is consistent with the Bi^{2+} location in the VRBE diagram. The holes released from Pr^{4+} or Tb^{4+} recombine with electrons at Bi^{2+} yielding Bi^{3+} A-band emission. The presence of Pr^{3+} and Tb^{3+} emission lines is explained because part of the energy of Bi^{3+} can be transferred to Pr^{3+} or Tb^{3+}, generating the 4f-4f emission[59-61]. The ET processes are further supported by the decreased decay lifetimes of the Bi^{3+} A-band emission in YPO_4:$0.005Bi^{3+}$,$0.005Pr^{3+}$ or Tb^{3+} as shown in Fig. S12.

Bi^{3+} acting as electron or as hole trap in this work is summarized in Table 3. In YPO_4:$0.005Bi^{3+}$,$0.005Ln^{3+}$ (Ln=Tb, and Pr) Bi^{3+} acts as deep electron trap and stable

recombination center. This is different from the garnets studied by Katayama et al. [37] where the CB-bottom is at lower VRBE leading to electron release from Bi^{2+}, see Table 1. The hole trapping depths of Tb^{3+} and Pr^{3+} can be engineered via changing x, leading to valence band lowering in $Y_{1-x}Lu_xPO_4$:0.005Bi^{3+},0.005Tb^{3+} or Pr^{3+} in Fig. 4.

Table 3. Bi^{3+} acting as electron (e^-) or as hole (h^+) trap in $REPO_4$:0.005Ln^{3+},0.005Bi^{3+} (RE=Y, Lu, and La) afterglow phosphors in the present work. The symbol h^+ means that holes release earlier from Tb^{4+}, Pr^{4+}, or Bi^{4+} than electrons from Bi^{2+}, Sm^{2+}, Tm^{2+}, Yb^{3+}, and Eu^{2+}.

Compound	h^+	transport	e^-
YPO_4	Tb^{3+} or Pr^{3+}	$h^+\rightarrow$	Bi^{3+}
$LuPO_4$	Tb^{3+} or Pr^{3+}	$h^+\rightarrow$	Bi^{3+}
$Y_{1-x}Lu_xPO_4$	Tb^{3+} or Pr^{3+}	$h^+\rightarrow$	Bi^{3+}
YPO_4	Bi^{3+}	$h^+\rightarrow$	Bi^{3+}
YPO_4	Bi^{3+}	$h^+\rightarrow$	Sm^{3+}
YPO_4	Bi^{3+}	$h^+\rightarrow$	Tm^{3+}
YPO_4	Bi^{3+}	$h^+\rightarrow$	Yb^{3+}
YPO_4	Bi^{3+}	$h^+\rightarrow$	Eu^{3+}
$Y_{1-x}Lu_xPO_4$	Bi^{3+}	$h^+\rightarrow$	Eu^{3+}
$LaPO_4$	Bi^{3+}	$h^+\rightarrow$	Eu^{3+}

In the TL glow curve of YPO_4:0.005Bi^{3+} in Fig. 6 and S3a, a glow peak I appears at ~416 K which shows Bi^{3+} $^3P_1\rightarrow{}^1S_0$ emission at 245 nm. In Ref [28] hole liberation from Bi^{4+} and recombination on Bi^{2+} was assigned to peak I in YPO_4, but in [2] we attributed the same TL-peak to hole release from an intrinsic defect. Below we will further motivate this latter assignment and motivate that peak IIIc is due to hole release from Bi^{4+}.

Glow peak I always appears strong in the presence of deep electron traps like Bi^{3+} (Fig. S3a), Eu^{3+} (Fig. 5), Sm^{3+} (Fig. S4 in [2]), and Yb^{3+} (Fig. S3i) and emission is then from the electron trapping centre. This already suggest that peak I is due to hole release. When another competing hole trap is present, peak I appears weaker as in YPO_4:Eu^{3+},Pr^{3+} or with Sm^{3+},Pr^{3+} in Fig. S4 in [2] which further indicates the hole trap nature of peak I.

4.2. Bi^{3+} as shallow hole trap and engineering its depth by valence band changing

The electron release from Sm^{2+}, or Tm^{2+} to the conduction band is known to take place at 718 K, or 591 K at a heating rate of 5 K/s in Ce^{3+} co-doped YPO_4 in Ref. [62]. In Fig. 6 we do not observe a TL-glow above 550 K when Sm^{3+} or Tm^{3+} is present in YPO_4. Apparently the electrons trapped on Sm^{2+} and Tm^{2+} have already disappeared due to recombination with holes released at lower temperature. Peak I we already attributed to hole release from an unknown defect, and therefore the remaining peak IIIc is attributed to hole release from Bi^{4+} that recombines with Bi^{2+}, Sm^{2+}, Tm^{2+}, or Eu^{2+} yielding Bi^{3+} $^3P_1\rightarrow{}^1S_0$, and Ln^{3+} 4f-4f emissions. Moreover, the emission of Bi^{3+} and Ln^{3+} can be further used to design new optical materials. For example, designing possible energy transfer processes from Bi^{3+} and Eu^{3+} to Nd^{3+} provides a new route to deliberate design of infrared bio-imaging probe, which will be published elsewhere.

The onset of the room temperature thermoluminescence excitation (TLE) spectrum of YPO_4:0.005Eu^{3+}, 0.005Bi^{3+} at 210-260 nm in Fig. 9 resembles the onset of the VB→Eu^{3+} charge transfer band of YPO_4:0.005Eu^{3+}. The lower TLE intensity at 210 nm is most likely due to an over estimated illumination intensity on the sample. During CT band excitation, electrons are excited from the valence band to the $4f^7$ ($^8S_{7/2}$) ground state of Eu^{2+} and holes are generated in the valence band which can then be trapped by Bi^{3+} to form Bi^{4+}. During TL readout, the holes release from Bi^{4+} and then recombine with Eu^{2+} and Bi^{2+} to yield Eu^{3+} 4f-4f emission and Bi^{3+} A-band emission.

The VRBE scheme of $REPO_4$ (RE=Y, and Lu) in Fig. 10 predicts that the VRBEs in the ground states of Bi^{3+} and Pr^{3+} are almost the same, and the temperature of the glow peak due to the hole release from Bi^{4+} and Pr^{4+} and recombination on Eu^{2+} would be almost the same too. The ~66 K shifting of peaks IIIb in $Y_{1-x}Lu_xPO_4$:0.005Eu^{3+},0.005Pr^{3+} was attributed to increased activation energy for the hole release from Pr^{4+} in Ref [2] as shown in Fig. 7b. With increasing x, a glow peak IIIc shift ~56 K also presents in $Y_{1-x}Lu_xPO_4$:0.005Eu^{3+},0.005Bi^{3+}, which is consistent with the above VRBE prediction. Like Pr^{3+}, we attribute the shift to the increased activation energy for hole release from Bi^{4+} and recombination on Eu^{2+}. The T_m of glow peak I, that was also attributed to hole release, is almost stationary with changing x. Apparently the VRBE in the responsible hole trap changes along with the changing VRBE at the VB-top which may suggest that the hole trap is somehow related to the anions in the host.

The stacked VRBE scheme of $LaPO_4$ in Fig. 10 predicts that Eu^{3+} is a 3.67 eV deep electron trap, while Bi^{3+} and Tb^{3+} act as 1.36, and 1.23 eV shallow hole trapping centers. It means that the temperature of the TL glow peak maximum due to hole release from Bi^{4+} or Tb^{4+} would be almost the same. Fig. 8 shows that, like Tb^{3+} for TL glow peak IIIa, Bi^{3+} also gives rise to a glow peak IIIc at 206 K. Glow peak IIIa at 240 K for $LaPO_4$:0.005Eu^{3+}, 0.005Tb^{3+} in Fig. 8 was attributed to hole release from Tb^{4+} in Lyu et. al [2]. We therefore tentatively assign glow peak IIIc at 206 K for $LaPO_4$:0.005Eu^{3+},0.005Bi^{3+} in Fig. 8 to hole release from Bi^{4+}. It corresponds with a trap depth of 0.54 eV as shown in column 4 of Table 2 which is ~0.8 eV smaller than the 1.36 eV predicted from VRBE scheme. A similar deviation with the VRBE prediction was observed for YPO_4:0.005Eu^{3+},0.005Pr^{3+} or Tb^{3+} [2] and for Eu^{3+},Pr^{3+}-, or Eu^{3+},Tb^{3+}-codoped $GdAlO_3$[14] it deviated ~0.3 eV. During the recombination phase the holes do not migrate at the top of the valence band but as trapped hole centers or V_k centers, and the lower activation energy is then attributed to the binding energy of the V_k center. The strong glow peak IIc just above room temperature in Fig. 8 for $LaPO_4$:0.005Eu^{3+},0.005Bi^{3+} is attributed to hole release from intrinsic hole trap(s) in $LaPO_4$.

5. Conclusions

Photoluminescence spectroscopy, the VRBE scheme, and thermally stimulated luminescence spectra were combined to study electron and hole capture in Bi^{3+} doped phosphors. We showed that Bi^{3+} can act both as electron and as hole trap in lanthanide co-doped rare earth ortho phosphates. In YPO_4:0.005Bi^{3+},0.005Ln^{3+} (Ln=Pr and Tb), the Ln^{3+} co-dopants are the shallow hole trapping centers, while Bi^{3+} acts as the deep electron trapping and the recombination center. The holes release from Ln^{4+} at lower temperature and

recombine through the valence band with Bi^{2+} to yield Bi^{3+} $^3P_1 \rightarrow {}^1S_0$ emission. For YPO_4: $0.005Ln^{3+}$,$0.005Bi^{3+}$ (Ln=Tm, Sm, Eu, and Yb), the Ln^{3+} co-dopants act as the deep electron trapping and recombination centers, while Bi^{3+} is the shallow hole trapping center. The holes release from Bi^{4+} at lower temperature than electrons from Ln^{2+} and recombine through valence band with Ln^{2+} to produce Ln^{3+} 4f-4f emission during TL-readout. The vacuum referred binding energy at the valence band top in $Y_{1-x}Lu_xPO_4$:$0.005Eu^{3+}$,$0.005Bi^{3+}$ can be lowered through changing x, and this leads to the increasing of the Bi^{3+} hole trap depth. By using Bi^{3+} as the shallow hole trap the recombination emission can be adjusted from the ultraviolet to the blue, or the red, or the infrared by varying the deep electron trap from Bi^{3+} to Tm^{3+} or to Sm^{3+} or Eu^{3+}, or Yb^{3+}. With deep understanding of Bi^{2+}, Bi^{3+} and lanthanide trap level locations, one may engineer the charge carrier trapping and release processes involving Bi. Combined with a lanthanide this provides a novel route to deliberate design of optical storage and afterglow materials, such as infrared bio-imaging probes.

6. Acknowledgements

T. Lyu acknowledges the Chinese Scholarship Council for his Ph.D. scholarship (Tianshuai Lyu: No. 201608320151). We would like to acknowledge fruitful discussions on afterglow phosphors and luminescence mechanisms with Dr Adrie J.J. Bos from Delft University of Technology.

Reference

1. K. Van den Eeckhout, D. Poelman and P. F. Smet, *Materials*, 2013, **6**, 2789-2818.
2. T. Lyu and P. Dorenbos, *Journal of Materials Chemistry C*, 2018, **6**, 369-379.
3. Y. Li, M. Gecevicius and J. Qiu, *Chemical Society Reviews*, 2016, **45**, 2090-2136.
4. H. Luo, A. J. J. Bos and P. Dorenbos, *The Journal of Physical Chemistry C*, 2017, **121**, 8760-8769.
5. T. Matsuzawa, Y. Aoki, N. Takeuchi and Y. Murayama, *Journal of the Electrochemical Society*, 1996, **143**, 2670-2673.
6. R. Kabe and C. Adachi, *Nature*, 2017, **550**, 384-387.
7. W. Fan, N. Lu, C. Xu, Y. Liu, J. Lin, S. Wang, Z. Shen, Z. Yang, J. Qu, T. Wang, S. Chen, P. Huang and X. Chen, *ACS Nano*, 2017, **11**, 5864-5872.
8. Z. Pan, Y.-Y. Lu and F. Liu, *Nat Mater*, 2012, **11**, 58-63.
9. Z. Li, Y. Zhang, X. Wu, L. Huang, D. Li, W. Fan and G. Han, *Journal of the American Chemical Society*, 2015, **137**, 5304-5307.
10. L. D. Hu, Y. Fan, L. Liu, X. M. Li, B. Z. Zhao, R. Wang, P. Y. Wang, A. M. El-Toni and F. Zhang, *Advanced Optical Materials*, 2017, **5**, 1700680.
11. F. Liu, W. Yan, Y.-J. Chuang, Z. Zhen, J. Xie and Z. Pan, *Scientific Reports*, 2013, **3**, 1554.
12. Y.-F. Liu, P. Liu, L. Wang, C.-E. Cui, H.-C. Jiang and J. Jiang, *Chemical Communications*, 2017, **53**, 10636-10639.
13. M. Thoms, H. von Seggern and A. Winnacker, *Physical Review B*, 1991, **44**, 9240-9247.
14. H. Luo, A. J. J. Bos and P. Dorenbos, *The Journal of Physical Chemistry C*, 2016, **120**, 5916-5925.
15. K. Chakrabarti, V. K. Mathur, J. F. Rhodes and R. J. Abbundi, *Journal of Applied Physics*, 1988, **64**, 1363-1366.
16. P. Dorenbos, *Physical Review B*, 2012, **85**, 165107.
17. P. Dorenbos, *Journal of Materials Chemistry*, 2012, **22**, 22344-22349.
18. P. Dorenbos, *ECS Journal of Solid State Science and Technology*, 2013, **2**, R3001-R3011.

19. R. H. P. Awater and P. Dorenbos, *Journal of Luminescence*, 2017, **184**, 221-231.
20. P. Boutinaud, *Inorganic Chemistry*, 2013, **52**, 6028-6038.
21. P. Boutinaud and E. Cavalli, *Chemical Physics Letters*, 2011, **503**, 239-243.
22. G. Blasse, A. Meijerink, M. Nomes and J. Zuidema, *Journal of Physics and Chemistry of Solids*, 1994, **55**, 171-174.
23. L. Li, M. Peng, B. Viana, J. Wang, B. Lei, Y. Liu, Q. Zhang and J. Qiu, *Inorganic Chemistry*, 2015, **54**, 6028-6034.
24. M. A. Hamstra, H. F. Folkerts and G. Blasse, *Journal of Materials Chemistry*, 1994, **4**, 1349-1350.
25. A. M. Srivastava, *Journal of Luminescence*, 1998, **78**, 239-243.
26. M. Peng and L. Wondraczek, *Opt. Lett.*, 2009, **34**, 2885-2887.
27. R. H. P. Awater and P. Dorenbos, *The Journal of Physical Chemistry C*, 2016, **120**, 15114-15118.
28. R. H. P. Awater, L. C. Niemeijer-Berghuijs and P. Dorenbos, *Optical Materials*, 2017, **66**, 351-355.
29. H.-T. Sun, J. Zhou and J. Qiu, *Progress in Materials Science*, 2014, **64**, 1-72.
30. J. L. DiMeglio and J. Rosenthal, *Journal of the American Chemical Society*, 2013, **135**, 8798-8801.
31. J. L. Tallon, R. G. Buckley, P. W. Gilberd, M. R. Presland, I. W. M. Brown, M. E. Bowden, L. A. Christian and R. Goguel, *Nature*, 1988, **333**, 153.
32. F. Kang, M. Peng, D. Y. Lei and Q. Zhang, *Chemistry of Materials*, 2016, **28**, 7807-7815.
33. G. Blasse and A. Bril, *Journal of Chemical Physics*, 1968, **48**, 217-222.
34. H. S. Kiliaan and G. Blasse, *Materials Chemistry and Physics*, 1987, **18**, 155-170.
35. A. M. Srivastava, *Materials Research Bulletin*, 2002, **37**, 745-751.
36. W. Sun, R. Pang, H. Li, D. Li, L. Jiang, S. Zhang, J. Fu and C. Li, *Journal of Materials Chemistry C*, 2017, **5**, 1346-1355.
37. Y. Katayama, A. Hashimoto, J. Xu, J. Ueda and S. Tanabe, *Journal of Luminescence*, 2017, **183**, 355-359.
38. Z. Zou, X. Tang, C. Wu, D. Wang, J. Zhang, Z. Ci, S. Du and Y. Wang, *Materials Research Bulletin*, 2018, **97**, 251-259.
39. Y. Katayama, J. Ueda and S. Tanabe, *Opt. Mater. Express*, 2014, **4**, 613-623.
40. D. D. Jia, J. Zhu and B. Q. Wu, *Journal of the Electrochemical Society*, 2000, **147**, 386-389.
41. Y. Jin, Y. Hu, L. Chen, X. Wang, G. Ju and Z. Mu, *Radiation Measurements*, 2013, **51-52**, 18-24.
42. W. Wang, Z. Sun, X. He, Y. Wei, Z. Zou, J. Zhang, Z. Wang, Z. Zhang and Y. Wang, *Journal of Materials Chemistry C*, 2017, **5**, 4310-4318.
43. T. Wang, X. Xu, D. Zhou, Y. Yang, J. Qiu and X. Yu, *Inorganic Chemistry*, 2016, **55**, 894-901.
44. S. Wang, W. Chen, D. Zhou, J. Qiu, X. Xu and X. Yu, *Journal of the American Ceramic Society*, 2017, **100**, 3514-3521.
45. S. Lai, Z. Yang, J. Liao, J. Qiu, Z. Song, Y. Yang and D. Zhou, *Materials Research Bulletin*, 2014, **60**, 714-718.
46. A. J. J. Bos, R. M. van Duijvenvoorde, E. van der Kolk, W. Drozdowski and P. Dorenbos, *Journal of Luminescence*, 2011, **131**, 1465-1471.
47. J. Ueda, P. Dorenbos, A. J. J. Bos, A. Meijerink and S. Tanabe, *The Journal of Physical Chemistry C*, 2015, **119**, 25003-25008.
48. A. M. Srivastava and S. J. Camardello, *Optical Materials*, 2015, **39**, 130-133.
49. E. Cavalli, F. Angiuli, F. Mezzadri, M. Trevisani, M. Bettinelli, P. Boutinaud and M. G. Brik, *J. Phys.-Condes. Matter*, 2014, **26**, 385503.
50. U. Sasum, M. Kloss, A. Rohmann, L. Schwarz and D. Haberland, *Journal of Luminescence*, 1997, **72-74**, 255-256.
51. E. Nakazawa and F. Shiga, *Journal of Luminescence*, 1977, **15**, 255-259.
52. D. Wang and Y. Wang, *Materials Research Bulletin*, 2007, **42**, 2163-2169.

53. R. Moncorge, G. Boulon and J. P. Denis, *Journal of Physics C-Solid State Physics*, 1979, **12**, 1165-1171.
54. S. W. S. McKeever, *Thermoluminescence of Solids*, Cambridge University Press, Cambridge, 1985.
55. R. Chen and S. A. A. Winer, *Journal of Applied Physics*, 1970, **41**, 5227-5232.
56. W. Hoogenstraaten, *Philips Res. Rep*, 1958, **13**, 515–693.
57. J. Ueda, P. Dorenbos, A. J. J. Bos, K. Kuroishi and S. Tanabe, *Journal of Materials Chemistry C*, 2015, **3**, 5642-5651.
58. R. H. P. Awater and P. Dorenbos, *Journal of Luminescence*, 2017, **188**, 487-489.
59. T. Jüstel, P. Huppertz, W. Mayr and D. U. Wiechert, *Journal of Luminescence*, 2004, **106**, 225-233.
60. F. Angiuli, E. Cavalli and A. Belletti, *Journal of Solid State Chemistry*, 2012, **192**, 289-295.
61. G. Blasse and A. Bril, *The Journal of Chemical Physics*, 1967, **47**, 1920-1926.
62. A. J. J. Bos, P. Dorenbos, A. Bessière and B. Viana, *Radiation Measurements*, 2008, **43**, 222-226.